AMERICAN JOURNAL OF PHYSIOLOGY
HEART AND CIRCULATORY PHYSIOLOGY

Am J Physiol Heart Circ Physiol 320: H1543–H1553, 2021.
First published February 19, 2021; doi:10.1152/ajpheart.00703.2020

RESEARCH ARTICLE

Muscle Mechanics and Ventricular Function

In vivo application and validation of a novel noninvasive method to estimate the end-systolic elastance

Stamatia Pagoulatou,[1] Karl-Philipp Rommel,[2,3] Karl-Patrik Kresoja,[2,3] Maximilian von Roeder,[2,3] Philipp Lurz,[2,3] Holger Thiele,[2,3] Vasiliki Bikia,[1] Georgios Rovas,[1] Dionysios Adamopoulos,[4] and Nikolaos Stergiopulos[1]

[1]*Laboratory of Hemodynamics and Cardiovascular Technology, Institute of Bioengineering, Ecole Polytechnique Fédérale de Lausanne, Lausanne, Switzerland;* [2]*Department of Cardiology, Heart Center Leipzig at University of Leipzig, Leipzig, Germany;* [3]*Leipzig Heart Institute, Leipzig, Germany; and* [4]*Cardiology Department, Geneva University Hospitals, Geneva, Switzerland*

Abstract

Accurate assessment of the left ventricular (LV) systolic function is indispensable in the clinic. However, estimation of a precise index of cardiac contractility, i.e., the end-systolic elastance (E_{es}), is invasive and cannot be established as clinical routine. The aim of this work was to present and validate a methodology that allows for the estimation of E_{es} from simple and readily available noninvasive measurements. The method is based on a validated model of the cardiovascular system and noninvasive data from arm-cuff pressure and routine echocardiography to render the model patient-specific. Briefly, the algorithm first uses the measured aortic flow as model input and optimizes the properties of the arterial system model to achieve correct prediction of the patient's peripheral pressure. In a second step, the personalized arterial system is coupled with the cardiac model (time-varying elastance model) and the LV systolic properties, including E_{es}, are tuned to predict accurately the aortic flow waveform. The algorithm was validated against invasive measurements of E_{es} (multiple pressure-volume loop analysis) taken from n = 10 patients with heart failure with preserved ejection fraction and n = 9 patients without heart failure. Invasive measurements of E_{es} (median = 2.4 mmHg/mL, range = [1.0, 5.0] mmHg/mL) agreed well with method predictions (normalized root mean square error = 9%, ρ = 0.89, bias = −0.1 mmHg/mL, and limits of agreement = [−0.9, 0.6] mmHg/mL). This is a promising first step toward the development of a valuable tool that can be used by clinicians to assess systolic performance of the LV in the critically ill.

NEW & NOTEWORTHY In this study, we present a novel model-based method to estimate the left ventricular (LV) end-systolic elastance (E_{es}) according to measurement of the patient's arm-cuff pressure and a routine echocardiography examination. The proposed method was validated in vivo against invasive multiple-loop measurements of E_{es}, achieving high correlation and low bias. This tool could be most valuable for clinicians to assess the cardiovascular health of critically ill patients.

cardiovascular modeling; inverse methods; left ventricular contractility; nonivasive monitoring; P-V loop

INTRODUCTION

Left ventricular (LV) contractility is a major determinant of the performance of the cardiovascular system (1). Its accurate assessment is of vital importance for the hemodynamic evaluation of the critically ill (2). In clinical practice, LV systolic function is often appreciated through the echocardiographic evaluation of LV volumes and particularly of the ejection fraction (EF), defined as the ratio of stroke volume (SV) over the end-diastolic volume (EDV). Despite its popularity, EF is in fact limited in offering a complete characterization of the cardiac inotropic state (3); it cannot (and should not) be interpreted without knowledge of preload and afterload. In addition, it confounds information on the cardiac structure (EDV), changes in which do not necessarily reflect on the level of contractility.

The gold standard method for assessing LV systolic function to date is the invasive measurement of LV pressure-volume (P-V) loops under varying load conditions from which the end-systolic pressure-volume relation (ESPVR) is extracted (4, 5). The ESPVR as described by its slope, i.e., the end-systolic elastance (E_{es}), and its volume axis intercept, i.e., the dead volume V_d, has been proven to be less load sensitive than other indices of ventricular contractility (6). For an increased E_{es}, the ventricle is able to eject more blood volume against the same afterload, which is indicative of increased contractility

Correspondence: S. Pagoulatou (stamatia.pagoulatou@epfl.ch).
Submitted 26 August 2020 / Revised 18 February 2021 / Accepted 18 February 2021

(5). The bedside use of E_{es} in the clinic is not, however, established due to the invasive and expensive nature of the P-V loop measurement. There is, therefore, a clear need of a method that will allow for the derivation of E_{es} from simple and readily available noninvasive measurements, such as echocardiography.

Recently, we proposed a noninvasive method to estimate E_{es} based on measurements of aortic flow, peripheral pressure, and EF (7). The method leverages a validated, one-dimensional (1-D) model of the systemic circulation (8) and works in an inverse problem-solving manner to derive an accurate description of the patient's arterial and cardiac properties. It was previously tested on a database of 50 virtual patients, yielding promising results (7).

Naturally, our next step is the in vivo validation of the noninvasive method's accuracy against invasively acquired E_{es} measures. To this aim, this paper presents an improved version of the original methodology. Subsequently, we demonstrate the performance of the updated noninvasive method against invasive P-V loop measurements acquired on a registry of patients with and without heart failure (HF).

METHODS

Description of the Model of the Cardiovascular System

The method uses a complete 1-D model of the arterial tree, comprising 103 arterial segments, whereby the Navier–Stokes equations are solved at each segment combined with a constitutive law for the wall elasticity (8). For a complete description of the mathematical model, the reader is referred to the original publication by Reymond et al. (8). Each terminal arterial segment is coupled with a three-element Windkessel model that accounts for the resistance and compliance of the terminal beds. As a proximal boundary condition, the model can receive two possible inputs: either we prescribe a measured aortic flow waveform [typically acquired via echocardiography or cardiac magnetic resonance imaging (CMR)] or the arterial tree is coupled with a varying elastance model describing the pumping function of the left ventricle.

Originally, the cardiac model consisted of a time-varying elastance function that assumes a linear LV P-V ratio at each time point. Recently, we updated the instantaneous LV P-V relation to include the nonlinearity of the end-diastolic pressure-volume relation (EDPVR). The P-V relation is now described as:

$$P_{LV}(V_{LV}) = \epsilon(t) \cdot \mathrm{ESPVR} + (1 - \epsilon(t)) \cdot \mathrm{EDPVR}$$

Where $\epsilon(t)$ is an activation function varying from 0 to 1, ESPVR is equal to $E_{es} \cdot (V_{LV} - V_d)$, and EDPVR is equal to $P_0 \cdot \exp(\beta \cdot V_{LV})$, with P_0 being the dead pressure and β a diastolic stiffness parameter.

Description of the Noninvasive Method to Derive E_{es}

The noninvasive method to estimate E_{es} and V_d uses a reverse-engineering approach and works in two steps (Fig. 1). In a first step, it optimizes the properties of the arterial tree according to the patient's age, height, heart rate, arm-cuff brachial systolic (bSBP) and diastolic (bDBP) pressure, echocardiographic aortic flow (LVOT), and diameter (Fig. 1*A*). This optimization technique was recently published (9) and was validated against in vivo data in terms of predicting the central pulse wave velocity and the central pressure. Briefly, we first adjust the geometry of the arterial tree by multiplying the diameter of each segment by a common factor γ_{geo} (equal to the ratio between the measured and model default aortic root diameter). Subsequently, we prescribe as input the echocardiography-derived proximal aortic flow waveform and tune the remaining model parameters, i.e., the compliance of each systemic artery, and the resistance and compliance of the terminal Windkessel models. The tuning of the arterial compliance curve is done to achieve the measured brachial pulse pressure. During this process, we account for the preferential stiffening of the proximal aorta with aging and, therefore, enforce increased proximal stiffness for older subjects (9). This entails the use of two stiffening factors, one local (proximal aortic) γ_{local} and one global γ_{global} (9). The latter factor is also used for the adjustment of the compliance of the terminal Windkessel models. The terminal resistance γ_{Rt} of the Windkessel models is tuned uniformly to achieve the measured mean pressure. At the end of each simulation, we compare the model-predicted brachial SBP and DBP with the measured values and correct the factors γ_{local}, γ_{global}, and γ_{Rt}, accordingly. The optimization yields an arterial tree that represents the patient's arterial load.

The second step uses the tuned arterial tree model and computes the patient's ESPVR. Figure 1*B* contains a schematic representation of this methodological step, which requires the additional echocardiographic measurement of the mitral valve inflow (namely, E-wave and A-wave), septal and lateral mitral annulus velocities (e'), LV end-diastolic (EDV), and end-systolic (ESV) volumes. The model input this time is the measured mitral flow waveform, which is calibrated to produce the measured stroke volume. To set up the simulation, we initially need to define the LV diastolic properties. To this aim, we approximate the end-diastolic pressure (EDP) based on literature expressions relating it with the echocardiographic average E/e' ratio (10) and then calculate the parameters of the exponential EDPVR, i.e., P_0 and β, following the single-beat method proposed by Klotz et al. (11) (the reader is referred to the original publication for methodological details). The only parameters remaining to be adjusted are the LV systolic properties, i.e., E_{es} and V_d. The simulation is launched first with arbitrary E_{es} and V_d and yields a prediction of the LV P-V loop and the flow at the proximal aorta. For a specific E_{es}, changes in V_d transpose the P-V loop horizontally (Fig. 2). Therefore, if the computed EDV does not correspond to the measured value, V_d is adjusted iteratively until convergence to the correct EDV (Figs. 1*B* and 2). When the intraventricular volumes are accurately predicted, the aortic flow waveform is compared to the measured LVOT flow curve. E_{es} is then changed in an external optimization loop until the LVOT flow waveform is accurately predicted (Figs. 1*B* and 2). The accuracy level for the EDV is set at ±1mL compared with the measurement, and for the aortic flow waveform, the area between the measured and model-derived curves is minimized until the error becomes smaller than 4% of the stroke volume.

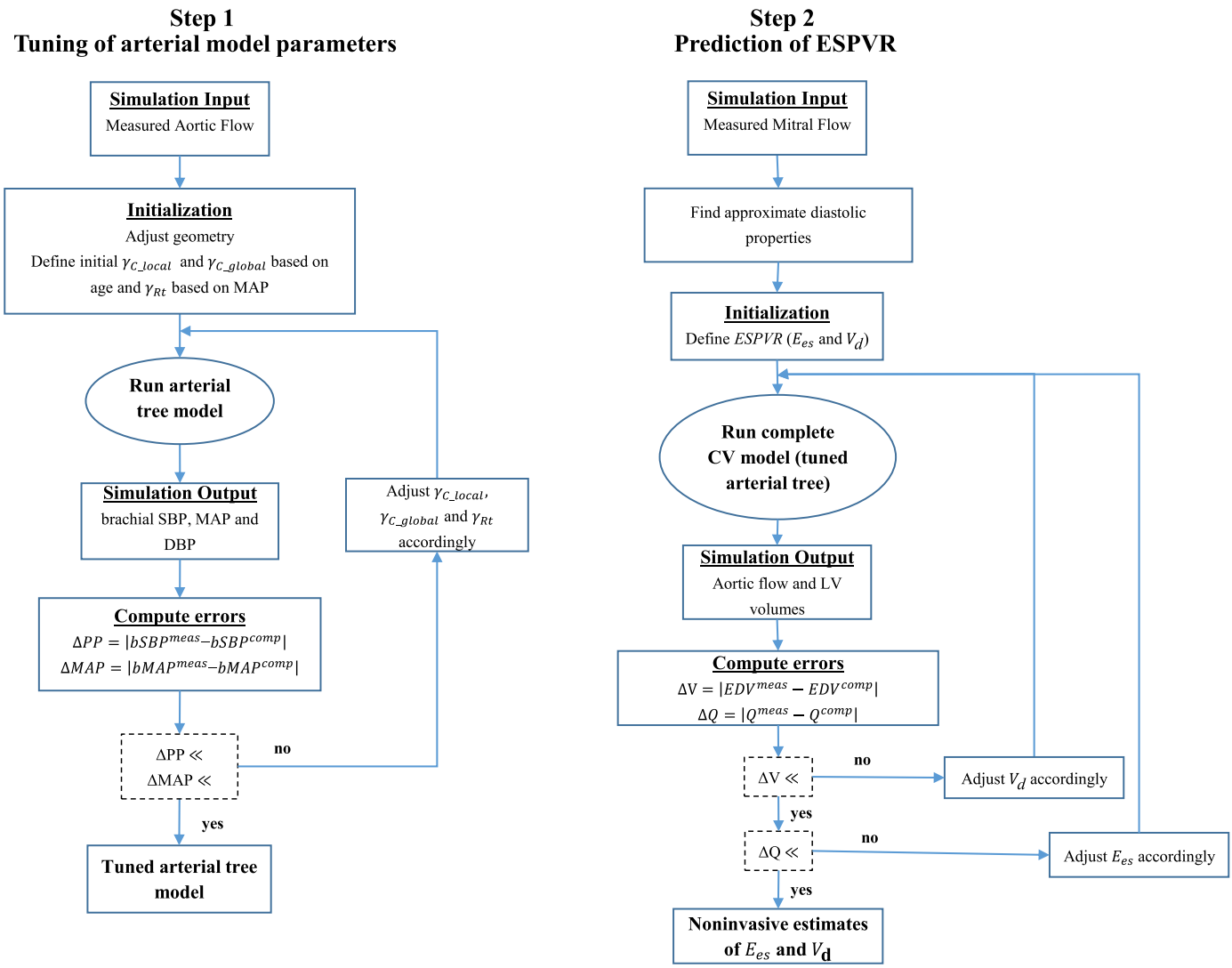

Figure 1. Two-step optimization algorithm to compute the end-systolic pressure-volume relation (ESPVR).

In Vivo Data

Study population.

The method was validated against invasive data acquired on patients at the Heart Center, Leipzig University, Germany, in the context of a previous study (12, 13). The study conforms to the principles outlined in the Declaration of Helsinki and received approval by the local ethics committee, and the participants gave informed written consent before inclusion in the study. The study population included a total of n = 19 patients, among which n = 10 had clinical and echocardiographic evidence for heart failure with preserved EF (HFpEF group) and n = nine had no HF symptoms (non-HF group). Patients with HFpEF were identified according to the guidelines of (14), using the following criteria: *1*) LVEF $\geq$ 50%, *2*) New York Heart Association functional class $\geq$II, and *3*) E/e' $\geq$15 or E/e' 8–15 combined with elevated *N*-terminal pro–B-type natriuretic peptide values (NT-proBNP >220 ng/L). The patient group without HF symptoms was referred for invasive coronary angiography but was free of any relevant coronary artery disease (CAD) (LVEF > 50%, E/e' <8, as well as normal values of NT-proBNP). Noninvasive classification according to the HF^{2}PEF score and the HFA-PEFF score demonstrated higher scores in the HFpEF cohort [HF^{2}PEF: 5 (interquartile range, IQR = 4–6) vs. 0 (0–1), $P < 0.01$; HFA-PEFF: 5 (IQR = 4–6) vs. 0 (0–2), $P < 0.01$]. According to the HF^{2}PEF and HFA-PEFF scores, an HFpEF diagnosis could be excluded in the non-HF group in 80% and 70% of cases, with a high noninvasive likelihood of an HFpEF diagnosis in the HF group in 30% and 70% of cases, respectively. However, the diagnosis was confirmed invasively in all patients with HF, as evidenced by elevated pulmonary capillary wedge pressure (PCWP) at rest ($\geq$15 mmHg) or during exercise ($\geq$25 mmHg), with non-HF patients demonstrating values below these cutoffs. Exclusion criteria included more than moderate valvular diseases or persistent atrial fibrillation. Further details on the study population can be found in previous articles (12, 13).

Magnetic resonance.

CMR was performed right before the invasive catheterization on an Intera 1.5-T scanner (Koninklijke Philips N.V., Amster-

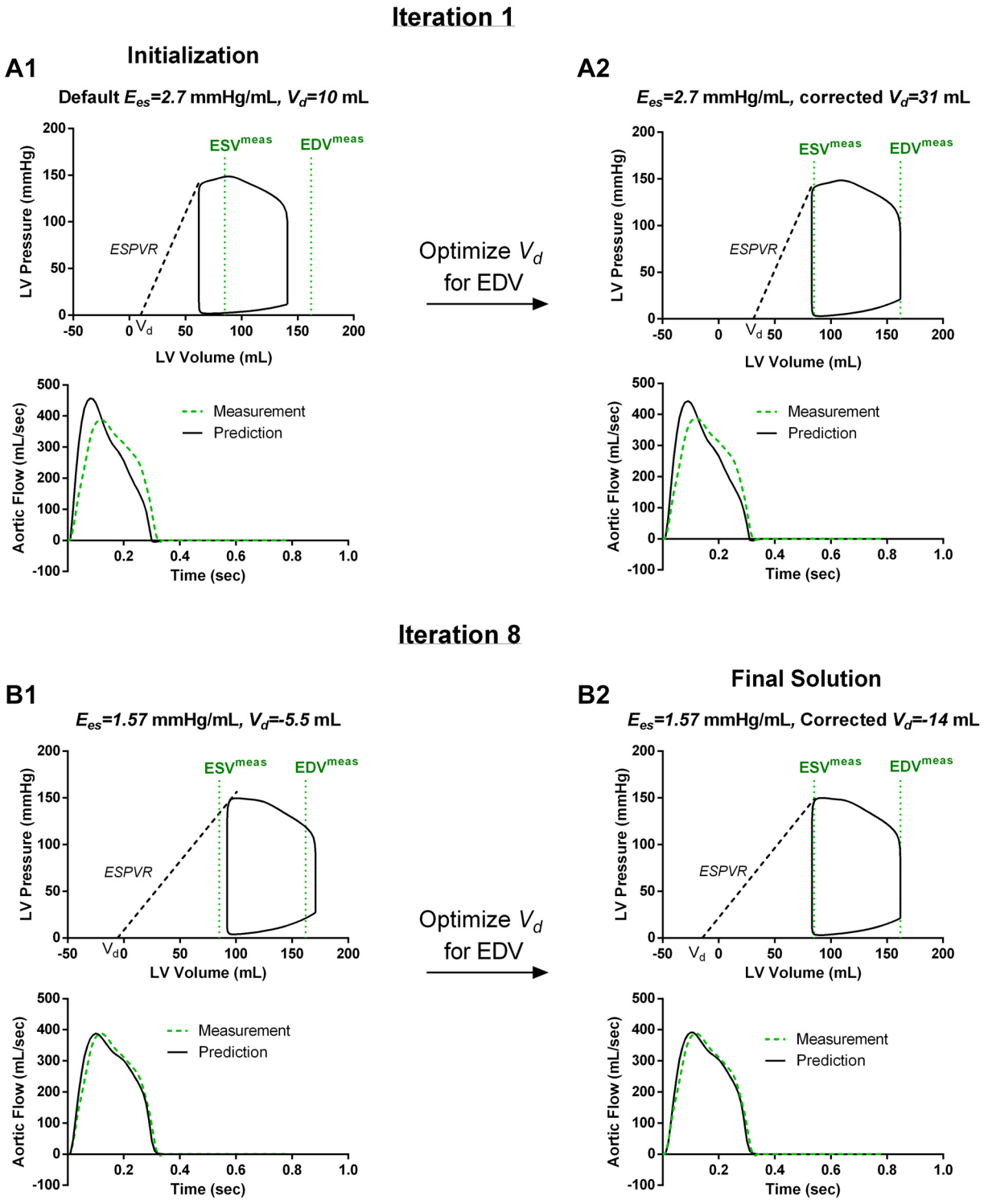

Figure 2. Example of the optimization process of the ESPVR for a specific HFpEF patient. *A1*: initialization of E_{es} and V_d. *A2*: optimization of V_d based on the measured EDV and update of the E_{es} based on the discrepancy of the model-derived and measured aortic flow. *B1*: beginning of 8th iteration with a new set of E_{es} and V_d. *B2*: convergence. EDV, end-diastolic volume; E_{es}, end-systolic elastance; ESPVR, end-systolic pressure-volume relation; HFpEF, heart failure with preserved ejection fraction; V_d, dead volume.

dam, the Netherlands). Patients were in the supine position and imaging was gated by ECG. Contiguous short-axis steady-state free precession sequences (SSFP) were obtained in two- and four-chamber views as well as a short-axis cine stack from the mitral valve annulus to the LV apex (T_R = 3.8 ms, T_E = 1.6 ms, 30 phases/cardiac cycle, 10-mm slice thickness). Image analysis was performed offline using commercially available software (CMR42, Circle Cardiovascular

Imaging Inc., Calgary, Alberta, Canada). LV volumes were computed after manually tracing the endocardial contours (12, 13). Stroke volume was calculated as the difference between the CMR-derived EDV and ESV, and EF was the ratio of the respective SV to EDV.

Cardiac catheterization protocol.

The detailed catheterization protocol is available in the original publications by Rommel et al. (12, 13). After exclusion of significant CAD, a 7-F conductance catheter (CD Leycom, Zoetermeer, the Netherlands) was introduced into the LV via right femoral artery access to record simultaneous LV P-V data. Subsequently, multiple LV P-V loops were recorded during reduction of the preload via transient occlusion of the inferior vena cava (inflation of an Amplatzer sizing balloon, St. Jude Medical, St. Paul, MN). Volume calibration was achieved by using the LV volumetric data from the CMR scan. The LV E_s was determined as the linear slope of the ESPVR and the V_d as its volume axis intercept. These measurements constitute the reference values. Similarly, the parameters of the exponential EDPVR were computed. The computations were performed by an experienced operator who was blinded to other test results (K.-P.R.).

Arm-cuff pressure.

Sphygmomanometric arm-cuff pressures were obtained at the mid brachial artery from a single measurement with automated BP monitors (Omron M300, Omron Healthcare, Kyoto, Japan, and Boso medicus uno, Boso, Jungingen, Germany) with the patient in the sitting position after 5 min of rest. Baseline systolic (bSBP) and diastolic (bDBP) pressures were recorded.

Echocardiography.

Echocardiographic exams were performed on a Vivid 9 system (General Electric Healthcare, Chalfont St. Giles, Great Britain). LVOT flow velocity was recorded with pulsed wave Doppler in the apical five-chamber view. The LVOT flow waveforms were then calibrated to produce the stroke volume measured with CMR (also used for calibration of invasive data). This was done due to lack of high-quality echocardiographic LV volume data. Aortic root diameter was captured in the parasternal long-axis view of the heart. Subsequently, mitral inflow pattern (E-wave and A-wave) were recorded in an apical four-chamber view along with the septal and lateral mitral valve annular velocities (e'). The average E/e' ratio was automatically computed. The mitral flow waveform was calibrated to produce the same measured stroke volume.

Method Implementation and Validation

The proposed methodology was implemented on the in vivo data of the n = 19 patients following the algorithm presented in Fig. 1. The model predictions for E_{es} and V_d were compared with the invasively acquired values. Since V_d is a measure of volume at a theoretical nonphysiological pressure, we also derived a characteristic LV end-systolic volume (V_{100}) at a given systolic pressure of 100 mmHg, as previously proposed in the literature (15). This volume index incorporates information on both E_{es} and V_d and is calculated as $V_{100} = \frac{100}{E_{es}} + V_d$. Model-predicted V_{100} values were also compared to the measurements.

Method Sensitivity

LV diastolic properties.

The methodology requires an approximation of the LV diastolic properties, namely, of the EDP and the parameters of the EDPVR (P_0 and β). As this can be a potential source of inaccuracy, we performed two analyses to understand how errors in the approximation of the EDP (and, consequently, in the LV diastolic properties P_0 and β) might undermine the method precision. In the first analysis, we investigated how E_{es}, V_d, and V_{100} predictions would be altered for a specific patient if EDP was underestimated and overestimated. Concretely, for this patient, the original approximation of EDP was 21 mmHg according to the measured E/e' ratio. We varied EDP at five levels, i.e., 5, 10, 15, 25, and 30 mmHg (16), and estimated the patient's systolic properties anew. In the second analysis, we assessed how E_{es}, V_d, and V_{100} predictions would change if we assumed a fixed EDP value of 15 mmHg for all study patients and repeated the optimization process. In this analysis, the respective P_0 and β parameters were set at physiological values to achieve the target EDP value.

Statistics

Statistical analysis was conducted using nonparametric tests, given the small sample size and the lack of data normality as visually confirmed. Continuous variables are presented as median (1st quartile, 3rd quartile) and categorical parameters as percentage. The correlation, accuracy, and bias between the model-predicted and invasive measurements of E_{es}, V_d, and V_{100} were evaluated by using Spearman's correlation coefficient (ρ), the root mean squared error normalized for the range (nRMSE), Bland–Altman analysis (mean difference $\bar{d}$, SD of differences, and limits of agreement LoA $= \bar{d} \pm 2$SD), and the intraclass correlation coefficient (ICC). Statistical differences between the HFpEF and non-HF patient groups were evaluated via the Mann–Whitney test. Statistical significance was set for P values lower than 0.05.

RESULTS

Table 1 summarizes the demographic and clinical characteristics of the 19 patients included in this study, i.e., 10 patients with HFpEF and nine patients without HF symptoms. Overall, the study population comprised older individuals (age median = 61 yr, 1st and 3rd quartile = 54 and 69 yr, respectively) as a result of the clinical indication for cardiac catheterization due to suspected critical cardiovascular diseases. The analysis included an equal number of women and men in total (9 vs. 10). The majority of patients had arterial hypertension (aHT) (68%) and normal EF (median = 61%, 1st and 3rd quartile = 52% and 66%, respectively).

Method Convergence

Figure 2 demonstrates how the second step of the methodology (presented in Fig. 1) converges to the E_{es} and V_d estimates for a specific patient with HFpEF. In the first iteration,

Table 1. *Descriptive and clinical characteristics of study population (n = 19 patients)*

Parameter	Total Sample	HFpEF Group	Non-HF Group	*P* Value
n	19	10	9	
Age, yr	61 (54, 69)	68 (60, 71)	57 (54, 61)	0.22
Sex, men/women	10/9	2/8	8/1	0.006*
Height, cm	170 (159, 179)	161 (158, 171)	178 (170, 183)	0.05*
Weight, kg	80 (76, 92)	80 (76, 88)	86 (79, 92)	0.56
BMI, kg/m^2	28.1 (25.8, 31.8)	31.7 (26.3, 33.5)	26.5 (25.7, 28.7)	0.15
BSA, m^2	1.98 (1.85, 2.12)	1.89 (1.84, 2.03)	2.10 (1.98, 2.14)	0.16
EF, %	61 (52, 66)	62 (54, 65)	56% (51, 66)	0.62
SBP, mmHg	155 (134, 164)	158 (151, 163)	155 (130, 164)	0.73
MAP, mmHg	108 (99, 110)	109 (100, 110)	100 (90, 110)	0.51
DBP, mmHg	82 (76, 85)	83 (81, 86)	80 (70, 84)	0.39
EDV, mL	126 (115, 148)	122 (111, 152)	143 (117, 145)	0.44
E_{es}, mL	2.4 (1.8, 2.9)	1.8 (1.6, 2.3)	2.9 (2.5, 3.0)	0.002*
V_d, mL	−7 (−28, 1)	−28 (−38, −11)	0 (−3, 8)	0.002*
V_{100}, mL	27 (19, 50)	22 (9, 43)	48 (24, 51)	0.16
EDP, mmHg	14 (12, 18)	18 (15, 21)	12 (11, 14)	0.002*
HR, beats/min	71 (67, 80)	70 (67, 76)	76 (68, 81)	0.31
aHT, %	68	80	55	0.35

Values are presented as median (1st, 3rd quartile). *Denotes statistically significant differences between the two groups. *P* values were produced using the Mann–Whitney test. aHT, arterial hypertension; BMI, body mass index; BSA, body surface area; DBP, brachial diastolic blood pressure; EDP, end-diastolic pressure; EDV, end-diastolic volume; E_{es}, end-systolic elastance; EF, ejection fraction; HF, heart failure; HFpEF, heart failure with preserved ejection fraction; HR, heart rate; MAP, mean arterial pressure; SBP, brachial systolic blood pressure; V_d, dead volume; V_{100}, end-systolic volume @ 100 mmHg.

E_{es} and V_d are initialized and the respective LV P-V loop and aortic flow waveform are computed (Fig. 2*A1*). In an internal optimization loop, V_d is adjusted so that the simulation yields the measured EDV (Fig. 2*A2*). After adjusting V_d, the model-predicted aortic flow wave shape still differs from the measured one; it has a higher maximal flow value and a steeper upstroke at early systole (Fig. 2*A2*). This discrepancy is due to the erroneous initialization of E_{es}. Subsequently, the aortic flow error is assessed and E_{es} is updated. After eight iterations, the algorithm converges to a solution for E_{es} and V_d, that is, when LV volumes and aortic flow waveform are accurately predicted (Fig. 2*B2*). For each case, convergence of the second methodological step was reached within 15 iterations on average.

In Vivo Validation

In Fig. 3, we compare the method predictions for E_{es}, V_d, and V_{100} against the invasive measurements. There was a high correlation between the estimated values and invasive measurements; ρ was 0.89, 0.74, and 0.94 for E_{es}, V_d, and V_{100}, respectively. In terms of accuracy, the proposed algorithm was able to predict all E_{es}, V_d, and V_{100} well; nRMSE was 9%, 13%, and 12%, respectively. For these indices, prediction had low bias ($\bar{d}$), narrow limits of agreement, and high ICCs, i.e., for E_{es}, $\bar{d} = -0.13$ mmHg/mL with SD = 0.37 mmHg/mL and ICC = 0.90; for V_d, $\bar{d} = -4$ mL with SD = 15 mL and ICC = 0.81; and for V_{100}, $\bar{d} = -4$ mL with SD = 9 mL and ICC = 0.91. We did not notice a statistically significant difference in the performance of the method between the HFpEF and the non-HF groups (for E_{es}, $\bar{d} = -0.04$ mmHg/mL with SD = 0.36 mmHg/mL for the HFpEF group and $\bar{d} = -0.23$ mmHg/mL with SD = 0.33 mmHg/mL for the non-HF group, *P* = 0.31).

Sensitivity to LV Diastolic Properties

Figure 4 demonstrates the accuracy of the estimation of EDP from the echocardiographic E/e' as previously proposed (10). Interestingly, we observe that E/e' is only fairly a reliable measure of EDP in this pressure range of [10, 24] mmHg. The overall correlation was poor, ρ = 0.5, nRMSE was 32%, and bias was 2.5 mmHg (LoA = [−6.1, 11.1] mmHg). The experimental relation between EDP and E/e' seemed to work better for the non-HF than the HFpEF group (Fig. 4).

To assess whether this level of accuracy in the EDP prediction is sufficient for the needs of our method, we conducted two analyses to appreciate its effect on the E_{es}, V_d, and V_{100} predictions. Figure 5 and Table 2 contain the results of the first analysis, in which we demonstrate how for a specific HFpEF, an overestimation and underestimation of EDP affect the method predictions. Originally, the EDP was estimated at 21 mmHg according to the echocardiographic measurement of E/e', and the model predicted the patient's P-V loop and aortic flow shown in Fig. 5 (with continuous lines). Then, EDP was varied at five discrete levels in the range of [5, 30] mmHg. Figure 5*B* shows the respective changes in the model-predicted aortic flow (dashed and dotted lines) for the two extreme EDP values, i.e., for EDP = 5 mmHg and EDP = 30 mmHg. We observe that the aortic flow waveform is only minimally affected by these drastic changes in EDP. Accordingly, the method-derived E_{es}, V_d, and V_{100} were minimally altered, as shown in Table 2.

In the second analysis, we supposed that EDP was equal to 15 mmHg for all patients and ran the algorithm anew. This caused only a minor increase in the nRMSE for the E_{es} prediction, namely, from 9% to 11%. Bias changed from −0.13 mmHg/mL to −0.18 mmHg/mL, the respective SD of differences from 0.37 mmHg/mL to 0.41 mmHg/mL and ICC from 0.90 to 0.87. This manipulation did not have any significant effect on the estimation of V_d or V_{100} either.

DISCUSSION

In this work, we present and validate a noninvasive method to estimate the LV ESPVR based on echocardiographic and

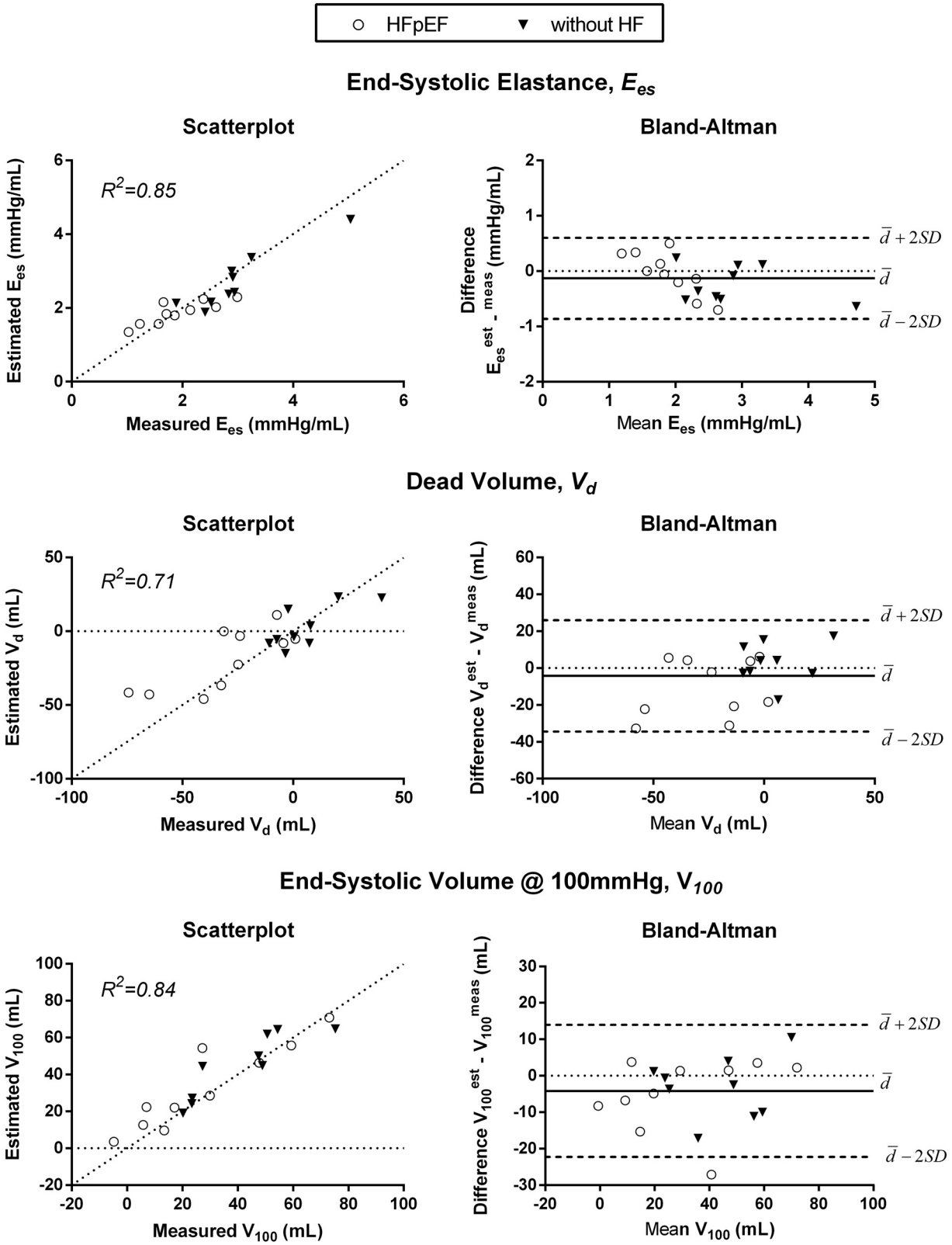

Figure 3. Scatterplots (*left*) and Bland–Altman plots (*right*) for E_{es} (*top*), V_d (*middle*), and V_{100} (*bottom*) as predicted by the method against invasive measurements (n = 19 patients). E_{es}, end-systolic elastance; V_d, dead volume; V_{100}, end-systolic volume @ 100 mmHg. HFpEF group, n = 10 patients; non-HF group, n = 9 patients.

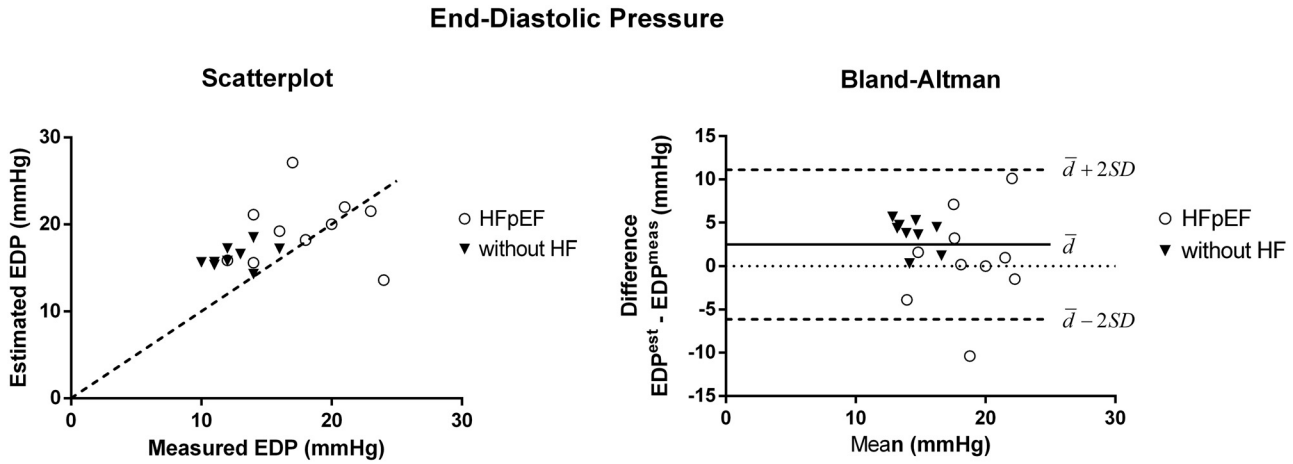

Figure 4. Scatterplot (*left*) and Bland–Altman plot (*right*) for the EDP approximated using its experimental correlation with E/e' (10) against invasive measurements ($n = 19$ patients). EDP, end-diastolic pressure. HFpEF group, $n = 10$ patients; non-HF group, $n = 9$ patients.

sphygmomanometric measurements. The basic concept relies on the fine-tuning of the properties of a generic, validated cardiovascular model to patient-specific standards. An original version of this methodology was previously described (7), where the proof of concept was demonstrated in silico. Since its original publication, the method has been upgraded to *1*) incorporate mechanisms of aging, according to the insights we have acquired from previous works (9, 17), and *2*) allow for the inclusion of different pathologies, such as diastolic dysfunction and hypertension.

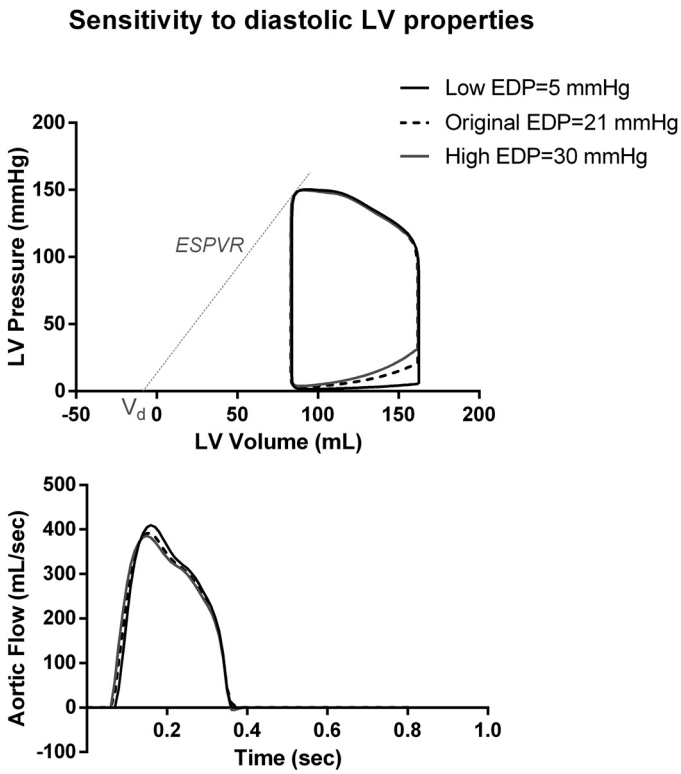

Figure 5. Method sensitivity to the estimated diastolic LV properties for a specific patient with HFpEF. *top*: LV P-V loops. *bottom*: aortic flow. HFpEF, heart failure with preserved ejection fraction; LV, left ventricular; P-V, pressure-volume.

Accordingly, we validated the presented method for patients with a critical cardiovascular disease, i.e., HFpEF, as well as for patients without HF symptoms. Overall, the method performed well when compared with in vivo acquired invasive data, achieving low bias and narrow limits of agreement. The errors were small for all ESPVR metrics, i.e., E_{es}, V_d, and V_{100}, and the predictions were equally precise for HFpEF and non-HF patients.

The success of the proposed method is largely due to the strong coupling between the measured quantities (brachial pressure and echocardiographic indices) and the functional properties of the heart and the arterial tree. In a previous computational study on the ventricular-arterial coupling (unpublished findings), we showed that changes in cardiac contractility have a direct and pronounced effect on central and peripheral hemodynamics even for an unchanged arterial load and cardiac output. Particularly, we reported that when LV contractility increases, the aortic flow wave shape changes, its upstroke becomes steeper, and its peak value increases, even if the stroke volume might be maintained. It is exactly this mechanism that we capture with the proposed algorithm, as shown in Fig. 2. In other words, the method is able to predict E_{es} accurately, because this information is contained in the measured aortic flow waveform that drives the optimization of the LV systolic properties. Consequently, accurate measurement of the aortic flow wave shape is vital to the method's accuracy.

A potential source of error is the definition of the LV diastolic properties in our simulations, which was based on the echocardiographic measurement of the E/e' ratio (10) and a previously developed methodology (11). Of course, the experimental relation relating EDP and E/e' has certain limitations (18) (as also highlighted in Fig. 4), and the overall technique might fail to yield accurate estimates of the EDPVR parameters. However, we demonstrated that this is not reflected in the accuracy of the E_{es} and V_d estimation; the method is not particularly sensitive to either EDP or parameters P_0 and β (Figs. 4 and 5, Table 2). This finding comes as no surprise if we take into account the

Table 2. *Method sensitivity to the approximation of the EDP*

	End-Systolic Elastance, E_{es}, mmHg/mL	Dead Volume, V_d, mL	End-Systolic Volume @ 100 mmHg, V_{100}, mL
Measurement	1.57	−4	59
Original estimation, EDP = 21 mmHg	1.56	−8	56
Estimation for different EDP levels			
EDP = 30 mmHg	1.65 (+6.0%)	−4	57 (+0.9%)
EDP = 25 mmHg	1.59 (+1.7%)	−8	55 (−2.2%)
EDP = 15 mmHg	1.37 (−12.1%)	−22	51 (−9.1%)
EDP = 10 mmHg	1.29 (−17.2%)	−29	49 (−13.5%)
EDP = 5 mmHg	1.13 (−27.6%)	−45	43 (−22.5%)

Results pertain to a specific HFpEF case. EDP, end-diastolic pressure; HFpEF, heart failure with preserved ejection fraction.

plethora of works (19–21) demonstrating that E_{es} is preload insensitive.

An important point is that we chose to change the original model for the EDPVR from linear to exponential. This was done to achieve a more comprehensive description of the LV diastolic properties. In fact, if we had described the EDPVR with just a constant slope, the method accuracy would not have been undermined (for E_{es}, nRMSE = 14% and $\bar{d} = -0.34$ mmHg/mL). Overall, we decided to integrate an exponential model here as this could serve as a solid basis for the additional prediction of the LV diastolic properties in the future.

Clinical Perspective

There are important implications to the application of this noninvasive methodology in the clinic. First, this tool can be implemented for the assessment of critically ill patients and for the prediction of personalized interventions in the ICU (13, 22, 23). A number of other clinical scenarios also could make use of our algorithm to accurately estimate the end-systolic elastance, such cardiac devices, or even coronary interventions (24).

An important point to consider is that the presented methodology does not characterize systolic function (i.e., E_{es}) alone but also offers a detailed representation of the afterload. This might allow for a more thorough investigation of the ventricular-arterial coupling (25) that goes beyond the traditional concept of the ratio of arterial over end-systolic elastance, E_a/E_{es}.

Therefore, there might be potential in applying the presented tool for effectively monitoring treatment effects in stable patients as well; particularly, in patients who have altered ventricular-arterial coupling with heightened afterload sensitivity, e.g., patients with aHT or HFpEF. This is of essence if we consider recent findings suggesting that hypercontractile phenotypes of patients with aHT and HFpEF are linked with adverse prognosis (26, 27).

Limitations and Future Steps

The reproducibility of the invasive P-V measurements was demonstrated in the previous work of Rommel et al. (13). A limitation of this work is that the LV volumes used for validation were taken from CMR measurements, although the method has been designed to use only echocardiographic volumes. This was done due to a lack of high-quality echocardiographic data of EDV and ESV. Previous studies suggest that EDV and ESV measured with noncontrast and contrast two-dimensional and three-dimensional echocardiography tend to be smaller and show greater variability than those measured with CMR (28). Therefore, there might be a nonnegligible bias when echocardiographic volumes are used instead. We acknowledge this limitation and plan to validate the method with echocardiographic data alone in the future. In addition, method results are likely to be influenced by errors in the measurement of the aortic flow wave shape.

It should be noted that the activation function used to describe the LV P-V relation might vary among different individuals, which could have an important impact on the results. In addition, cardiac contractility was described in the present work by using the time-varying elastance function. More detailed finite-element models exist (29, 30) that couple cavity mechanics with sarcomere mechanics. The use of such models might be relevant for the purposes of our method. Other model-related limitations are acknowledged in our previous publication (8).

The proposed algorithm cannot be applied to any patient without prior knowledge of the condition of his/her aortic valve. Strategically in this study, we chose to conduct the validation on patients free from any severe valve diseases. In the presence of severe aortic valve stenosis, aortic hemodynamics and particularly aortic flow wave shape are altered, as we previously demonstrated (31). Therefore, if we do not integrate an existing valvular pathology into the model, the method will fail to correctly predict the LV ESPVR. Accordingly, significant valvular diseases should be introduced into the simulation in advance. Given that during echocardiographic examination, clinicians usually assess valve condition, we assume that such information would be in general available.

In addition, the model was developed and validated for a healthy young adult (8, 32) and has been adapted to include the effects of normal aging (17). Consequently, the method has been developed to adjust the model parameters according to average trends expected in adults, without comprising effects of certain diseases, such as CAD. It would be meaningful to investigate different pathologies to have a better understanding of their modeling implications and ultimately achieve a more faithful representation of the cardiovascular properties of each patient. It would also be beneficial to assess the method's ability to capture expected changes in E_{es} due to inotropic drugs or differences between patient groups, such as systolic HF patients, dilated or hypertrophic myocardiopathy patients, etc.

Finally, we should note that the present methodology allows for the calculation of additional parameters of systolic

function, such as the maximal elastance, E_{max}, and its timing, t_{max}. This is an interesting potential, given that abnormal t_{max} values might be indicative of impaired systolic function, as highlighted in previous literature (33).

CONCLUSIONS

In this study, we described and validated a method that allows for the noninvasive estimation of the ESPVR in patients based on a few measurements that are usually conducted in routine cardiology, i.e., echocardiography and sphygmomanometry. This was motivated by the obvious fact that such a method would be a most valuable tool for clinicians to achieve accurate cardiac monitoring and optimize patient management. The validation of the proposed algorithm against invasive measurements of P-V loops demonstrated its accuracy and robustness. We concluded that the method performance depends mostly on the precision of the echocardiographic flow data. Method accuracy should be further investigated under different settings and for various diseases.

GRANTS

This study was funded by a research grant from the Heart Center, Leipzig.

DISCLOSURES

No conflicts of interest, financial or otherwise, are declared by the authors.

AUTHOR CONTRIBUTIONS

S.P. and N.S. conceived and designed research; K.-P.R., K.-P.K., M.v.R., P.L., and H.T. performed experiments; S.P., K.-P.R., K.-P.K., M.v.R., P.L., and H.T. analyzed data; S.P., N.S., K.-P.R., K.-P.K., M.v.R., P.L., H.T., and D.A. interpreted results of experiments; S.P. prepared figures and drafted manuscript; N.S., K.-P.R., K.-P.K., M.v.R., P.L., H.T., V.B., G.R., and D.A. edited and revised manuscript; S.P., N.S., K.-P.R., K.-P.K., M.v.R., P.L., H.T., V.B., G.R., and D.A. approved the final version of the manuscript.

REFERENCES

1. **Cecconi M**, **De Backer D**, **Antonelli M**, **Beale R**, **Bakker J**, **Hofer C**, **Jaeschke R**, **Mebazaa A**, **Pinsky MR**, **Teboul JL**, **Vincent JL**, **Rhodes A.** Consensus on circulatory shock and hemodynamic monitoring. Task force of the European Society of Intensive Care Medicine. *Intensive Care Med* 40: 1795–1815, 2014. doi:10.1007/s00134-014-3525-z.
2. **Ochagavía A**, **Zapata L**, **Carrillo A**, **Rodríguez A**, **Guerrero M**, **Ayuela JM.** Evaluation of contractility and postloading in the intensive care unit. *Med Intensiva* 36: 365–374, 2012. doi:10.1016/j.medine.2012.07.007.
3. **Konstam MA**, **Abboud FM.** Ejection fraction: misunderstood and over-rated (changing the paradigm in categorizing heart failure). *Circulation* 135: 717–719, 2017. doi:10.1161/CIRCULATIONAHA.116.025795.
4. **Sagawa K**, **Suga H**, **Shoukas AA**, **Bakalar KM.** End-systolic pressure/volume ratio: a new index of ventricular contractility. *Am J Cardiol* 40: 748–753, 1977. doi:10.1016/0002-9149(77)90192-8.
5. **Suga H**, **Sagawa K.** Instantaneous pressure-volume relationships and their ratio in the excised, supported canine left ventricle. *Circ Res* 35: 117–126, 1974. doi:10.1161/01.res.35.1.117.
6. **Paley HW**, **McDonald IG**, **Blumenthal J**, **Mailhot J.** The effects of posture and isoproterenol on the velocity of left ventricular contraction in man. The reciprocal relationship between left ventricular volume and myocardial wall force during ejection on mean rate of circumferential shortening. *J Clin Invest* 50: 2283–2294, 1971. doi:10.1172/JCI106726.
7. **Pagoulatou SZ**, **Stergiopulos N.** Estimating left ventricular elastance from aortic flow waveform, ventricular ejection fraction, and brachial pressure: an in silico study. *Ann Biomed Eng* 46: 1722–1735, 2018. doi:10.1007/s10439-018-2072-0.
8. **Reymond P**, **Merenda F**, **Perren F**, **Rüfenacht D**, **Stergiopulos N.** Validation of a one-dimensional model of the systemic arterial tree. *Am J Physiol Heart Circ Physiol* 297: H208–H222, 2009. doi:10.1152/ajpheart.00037.2009.
9. **Pagoulatou SZ**, **Bikia V**, **Trachet B**, **Papaioannou TG**, **Protogerou AD**, **Stergiopulos N.** On the importance of the nonuniform aortic stiffening in the hemodynamics of physiological aging. *Am J Physiol Heart Circ Physiol* 317: H1125–H1133, 2019. doi:10.1152/ajpheart.00193.2019.
10. **Ommen SR**, **Nishimura RA**, **Appleton CP**, **Miller FA**, **Oh JK**, **Redfield MM**, **Tajik AJ.** Clinical utility of Doppler echocardiography and tissue Doppler imaging in the estimation of left ventricular filling pressures: a comparative simultaneous Doppler-catheterization study. *Circulation* 102: 1788–1794, 2000. doi:10.1161/01.CIR.102.15.1788.
11. **Klotz S**, **Hay I**, **Dickstein ML**, **Yi G-H**, **Wang J**, **Maurer MS**, **Kass DA**, **Burkhoff D.** Single-beat estimation of end-diastolic pressure-volume relationship: a novel method with potential for noninvasive application. *Am J Physiol Heart Circ Physiol* 291: H403–H412, 2006. doi:10.1152/ajpheart.01240.2005.
12. **Rommel K-P**, **von Roeder M**, **Oberueck C**, **Latuscynski K**, **Besler C**, **Blazek S**, **Stiermaier T**, **Fengler K**, **Adams V**, **Sandri M**, **Linke A**, **Schuler G**, **Thiele H**, **Lurz P.** Load-independent systolic and diastolic right ventricular function in heart failure with preserved ejection fraction as assessed by resting and handgrip exercise pressure–volume loops. *Circ Heart Fail* 11: e004121, 2018. doi:10.1161/CIRCHEARTFAILURE.117.004121.
13. **Rommel K-P**, **von Roeder M**, **Latuscynski K**, **Oberueck C**, **Blazek S**, **Fengler K**, **Besler C**, **Sandri M**, **Lücke C**, **Gutberlet M**, **Linke A**, **Schuler G**, **Lurz P.** Extracellular volume fraction for characterization of patients with heart failure and preserved ejection fraction. *J Am Coll Cardiol* 67: 1815–1825, 2016. doi:10.1016/j.jacc.2016.02.018.
14. **Paulus WJ**, **Tschöpe C**, **Sanderson JE**, **Rusconi C**, **Flachskampf FA**, **Rademakers FE**, **Marino P**, **Smiseth OA**, **De Keulenaer G**, **Leite-Moreira AF**, **Borbély A**, **Edes I**, **Handoko ML**, **Heymans S**, **Pezzali N**, **Pieske B**, **Dickstein K**, **Fraser AG**, **Brutsaert DL.** How to diagnose diastolic heart failure: a consensus statement on the diagnosis of heart failure with normal left ventricular ejection fraction by the Heart Failure and Echocardiography Associations of the European Society of Cardiology. *Eur Heart J* 28: 2539–2550, 2007. doi:10.1093/eurheartj/ehm037.
15. **Ky B**, **French B**, **May Khan A**, **Plappert T**, **Wang A**, **Chirinos JA**, **Fang JC**, **Sweitzer NK**, **Borlaug BA**, **Kass DA**, **St John Sutton M**, **Cappola TP.** Ventricular-arterial coupling, remodeling, and prognosis in chronic heart failure. *J Am Coll Cardiol* 62: 1165–1172, 2013. doi:10.1016/j.jacc.2013.03.085.
16. **ten BEA**, **Bertini M**, **Klautz RJ**, **Antoni ML**, **Holman ER**, **Nr van de V**, **Bax JJ**, **Steendijk P.** Noninvasive estimation of left ventricular filling pressures in patients with heart failure after surgical ventricular restoration and restrictive mitral annuloplasty. *J Thorac Cardiovasc Surg* 140: 807–815, 2010. doi:10.1016/j.jtcvs.2009.11.039.
17. **Pagoulatou S**, **Stergiopulos N.** Evolution of aortic pressure during normal ageing: a model-based study. *PloS One* 12: e0182173, 2017. doi:10.1371/journal.pone.0182173.
18. **Previtali M**, **Chieffo E**, **Ferrario M**, **Klersy C.** Is mitral E/E′ ratio a reliable predictor of left ventricular diastolic pressures in patients without heart failure? *Eur J Echocardiogr* 13: 588–595, 2012. doi:10.1093/ejechocard/jer286.
19. **Chen C-H**, **Fetics B**, **Nevo E**, **Rochitte CE**, **Chiou K-R**, **Ding P-A**, **Kawaguchi M**, **Kass DA.** Noninvasive single-beat determination of left ventricular end-systolic elastance in humans. *J Am Coll Cardiol* 38: 2028–2034, 2001. doi:10.1016/S0735-1097(01)01651-5.
20. **Senzaki H**, **Chen CH**, **Kass DA.** Single-beat estimation of end-systolic pressure-volume relation in humans. A new method with the potential for noninvasive application. *Circulation* 94: 2497–2506, 1996. doi:10.1161/01.cir.94.10.2497.

21. **Shishido T**, **Hayashi K**, **Shigemi K**, **Sato T**, **Sugimachi M**, **Sunagawa K.** Single-beat estimation of end-systolic elastance using bilinearly approximated time-varying elastance curve. *Circulation* 102: 1983–1989, 2000. doi:10.1161/01.cir.102.16.1983.
22. **Borlaug BA**, **Paulus WJ.** Heart failure with preserved ejection fraction: pathophysiology, diagnosis, and treatment. *Eur Heart J* 32: 670–679, 2011. doi:10.1093/eurheartj/ehq426.
23. **Kawaguchi M**, **Hay I**, **Fetics B**, **Kass DA.** Combined ventricular systolic and arterial stiffening in patients with heart failure and preserved ejection fraction. *Circulation* 107: 714–720, 2003. doi:10.1161/01.CIR.0000048123.22359.A0.
24. **Bastos MB**, **Burkhoff D**, **Maly J**, **Daemen J**, **den Uil CA**, **Ameloot K**, **Lenzen M**, **Mahfoud F**, **Zijlstra F**, **Schreuder JJ**, **Van Mieghem NM.** Invasive left ventricle pressure–volume analysis: overview and practical clinical implications. *Eur Heart J* 41: 1286–1297, 2020. doi:10.1093/eurheartj/ehz552.
25. **Chirinos JA.** Ventricular-arterial coupling: invasive and non-invasive assessment. *Artery Res* 7: 10, 2013. doi:10.1016/j.artres.2012.12.002.
26. **Lurz P**, **Kresoja K-P**, **Rommel K-P**, **von Roeder M**, **Besler C**, **Lücke C**, **Gutberlet M**, **Schmieder RE**, **Mahfoud F**, **Thiele H**, **Desch S**, **Fengler K.** Changes in stroke volume after renal denervation. *Hypertension* 75: 707–713, 2020. doi:10.1161/HYPERTENSIONAHA.119.14310.
27. **Wehner GJ**, **Jing L**, **Haggerty CM**, **Suever JD**, **Leader JB**, **Hartzel DN**, **Kirchner HL**, **Manus JNA**, **James N**, **Ayar Z**, **Gladding P**, **Good CW**, **Cleland JGF**, **Fornwalt BK.** Routinely reported ejection fraction and mortality in clinical practice: where does the nadir of risk lie? *Eur Heart J* 41: 1249–1257, 2020. doi:10.1093/eurheartj/ehz550.
28. **Wood PW**, **Choy JB**, **Nanda NC**, **Becher H.** Left ventricular ejection fraction and volumes: it depends on the imaging method. *Echocardiography* 31: 87–100, 2014. doi:10.1111/echo.12331.
29. **Kerckhoffs RCP**, **Neal ML**, **Gu Q**, **Bassingthwaighte JB**, **Omens JH**, **McCulloch AD.** Coupling of a 3D finite element model of cardiac ventricular mechanics to lumped systems models of the systemic and pulmonic circulation. *Ann Biomed Eng* 35: 1–18, 2007. doi:10.1007/s10439-006-9212-7.
30. **Lumens J**, **Delhaas T**, **Kirn B**, **Arts T.** Three-wall segment (TriSeg) model describing mechanics and hemodynamics of ventricular interaction. *Ann Biomed Eng* 37: 2234–2255, 2009. doi:10.1007/s10439-009-9774-2.
31. **Pagoulatou S**, **Stergiopulos N**, **Bikia V**, **Rovas G**, **Licker M-J**, **Müller H**, **Noble S**, **Adamopoulos D.** Acute effects of transcatheter aortic valve replacement on the ventricular-aortic interaction. *Am J Physiol Heart Circ Physiol* 319: H1451–H1458, 2020. doi:10.1152/ajpheart.00451.2020.
32. **Reymond P**, **Bohraus Y**, **Perren F**, **Lazeyras F**, **Stergiopulos N.** Validation of a patient-specific one-dimensional model of the systemic arterial tree. *Am J Physiol Heart Circ Physiol* 301: H1173–H1182, 2011. doi:10.1152/ajpheart.00821.2010.
33. **Scruggs SB**, **Hinken AC**, **Thawornkaiwong A**, **Robbins J**, **Walker LA**, **de Tombe PP**, **Geenen DL**, **Buttrick PM**, **Solaro RJ.** Ablation of ventricular myosin regulatory light chain phosphorylation in mice causes cardiac dysfunction in situ and affects neighboring myofilament protein phosphorylation. *J Biol Chem* 284: 5097–5106, 2009. doi:10.1074/jbc.M807414200.